Manuscript prepared for The Cryosphere Discuss.
with version 2014/09/16 7.15 Copernicus papers of the LaTeX class copernicus.cls.
Date: 29 January 2016

Modelling ~~the dynamic response of~~ calving front dynamics using a Level-Set Method: Application to Jakobshavn Isbræ, West Greenland~~, to calving rate perturbations~~

J.H. Bondzio[1], H. Seroussi[2], M. Morlighem[3], T. Kleiner[1], M. Rückamp[1], A. Humbert[1,4], and E. Larour[2]

[1]Alfred Wegener Institute, Helmholtz Centre for Polar and Marine Research, Bremerhaven, Germany
[2]Jet Propulsion Laboratory - California Institute of Technology, Pasadena, CA, USA
[3]Department of Earth System Science, University of California Irvine, Irvine, CA, USA
[4]University of Bremen, Bremen, Germany

Correspondence to: Johannes H. Bondzio (jbondzio@uci.edu)

Abstract

Calving is a major ~~means~~ mechanism of ice discharge of the Antarctic and Greenland Ice Sheets~~. The breaking off of icebergs changes the ice front configuration of marine terminating glaciers, which affects the~~, and a change in calving front position affects the entire stress regime of ~~their upstream areas. Recent observations show the close correlation between the ice front position and the behaviour of many outlet glaciers. However, modelling of a glacier subject to calving poses various challenges. No universal calving rate parametrisation is known, and tracking of a moving ice front and the related boundary conditions in~~ marine terminating glaciers. The representation of calving front dynamics in a two or three ~~spatial dimensions is~~ dimensional ice sheet model remains non-trivial. Here, we present the theoretical and technical framework for a Level-Set Method, an implicit boundary tracking scheme, which we ~~implemented~~ implement into the Ice Sheet System Model (ISSM). ~~The~~ This scheme allows us to study the dynamic response of a drainage basin to user-defined ~~front ablation~~ calving rates. We apply the method ~~in a suite of experiments~~ to Jakobshavn Isbræ, a major marine terminating outlet glacier of the western Greenland Ice Sheet. The model robustly reproduces the high sensitivity of the glacier to ~~frontal ablation in form of calving. We~~ calving, and we find that enhanced calving ~~is able to trigger~~ triggers significant acceleration of the ice stream. Upstream acceleration is sustained through a combination of ~~various feedback~~ mechanisms. However, both lateral stress and ice influx ~~into the trough are able to~~ stabilise the ice stream. This study ~~contributes to the present discussion on causes and effects of the continued~~ provides new insights into the ongoing changes occurring at Jakobshavn Isbræ, and emphasises that the incorporation of ~~seasonal calving~~ moving boundaries and dynamic lateral effects, not captured in flowline models, is key for realistic model projections of ~~future global~~ sea level rise on centennial time scales.

1 Introduction

Calving of icebergs is a major mean of ice discharge for marine terminating glaciers around the world. It accounts for about ~~50%~~ half of the ice discharge of the Greenland and Antarctic Ice Sheets (Cuffey and Paterson, 2010; Rignot et al., 2013). ~~Calving causes ice~~ This process causes calving front retreat, which leads to reduced basal and lateral stress and results in upstream flow acceleration.

[Figure 1 about here.]

~~Understanding calving dynamics remains challenging because of the diversity of factors that can trigger calving events. Bathymetry, tides and storm swell, as well as sea ice cover and temperatures of both sea water and air are possible factors influencing calving rates. However, their effect, their respective share and their interplay seem to vary from glacier to glacier, and is not well understood. Therefore, no universal calving rate parametrisation, which can be used in macroscopic ice sheet models, exists to date (Benn et al., 2007; Cuffey and P~~

In order to assess the impact of calving on the dynamics of ~~an outlet glacier~~outlet glaciers using an ice sheet model, we need to ~~implement boundary conditions at the dynamically evolving ice~~ include a dynamically evolving calving front. This ~~poses a second technical challenge as the ice front position needs to be tracked, and the related boundary conditions need to be updated accordingly.~~ requires tracking the calving front position and adjusting the boundary conditions accordingly. Addressing these issues is rather straightforward for 1D-flowline or 2D-flowband models (Nick et al., 2009; Vieli and Nick, 2011), where the ~~ice front can be~~ calving front is tracked along the ~~floor line~~flowline. However, this type of ~~models~~ model lacks the consistent representation of ~~mechanisms like lateral momentum transport and ice influx of converging ice streams~~lateral momentum transfer and lateral ice influx from tributaries for example, which have to be parametrised instead. This parametrisation may neglect feedback effects important for simulations on decadal to centennial time scales, e.g. catchment area entrainment (Larour et al., 2012a).

~~Therefore, it is desirable to implement~~ It is therefore critical to include a front tracking scheme in 2D-horizontal and 3D models, which has been addressed by only a few ice sheet models ~~only, e. g. Winkelmann et al. (2011).~~ (e.g. Jouvet et al., 2008; Winkelmann et al., 2011). Various approaches to model the evolution of the shape of ice exist. Explicit methods track the position of a set of points, which represent the ~~ice~~ calving front. They require a complex technical framework to allow for geometric operations like folding and intersection of the continuum boundary, tracking singularities in curvature, and determining the position of a point in space relative to the modelled continuum. ~~On the other hand, a suite of implicit boundary tracking methods exists, e.g.~~ Alternatively, the Level-Set Method ~~(LSM) by Osher and Sethian (1988). The LSM~~ (LSM Osher and Sethian, 1988) represents the continuum boundary implicitly by a contour, or “level-set”, of a ~~scalar valued~~ so-called “Level-Set Function” (LSF). It easily handles topological changes of the modelled continuum, like splitting and merging~~of its parts. It is well suited for the use in a parallel architecture, since it is~~. The LSM is based on a partial differential equation ~~. This allows for application to large~~ similar to the mass transport equation solved by ice sheet models. This makes the method straightforward to implement, and allows for the application to continental scale ice sheet simulations. ~~The method~~ Although the method does not necessarily conserve volume accurately, it is well established in Continuum Fluid Mechanics (Chang et al., 1996; Groß et al., 2006)~~, and can be used with various numerical schemes, like the Finite Differences Method or the Finite Element Method (FEM)~~. A LSM has been applied to ice flow modelling in test cases (Pralong and Funk, 2004), but not to real ice sheets yet.

Understanding calving dynamics remains challenging because of the diversity of factors involved in calving events. Bathymetry, tides and storm swell, as well as sea ice cover and temperatures of both sea water and air are possible factors influencing calving rates. However, their effect, their respective share and their interplay seem to vary from glacier to glacier, and are not well understood (Cuffey and Paterson, 2010). Therefore, no universal calving rate parametrisation exists to date (Benn et al., 2007), and we rely here on user-defined calving rates. However, incorporating calving rate parametrisations in the LSM is straightforward.

Jakobshavn Isbræ is a major marine terminating glacier in West Greenland, which drains about 6.5% of the Greenland Ice Sheet (Zwally et al., 2011). It is characterised by two ~~tributaries~~branches, which today terminate into ~~an ice-choked fjord of about~~ a 30 km ~~length~~ long ice-choked fjord (Figs. 1 and 2). The southern ~~tributary~~ branch exhibits high flow velocities, which are confined to a narrow, deep trough of about 5 km width. The trough retrogradely slopes inland to a maximum depth of about 1700 m below sea level (Gogineni et al., 2014)~~. It~~, and discharges most of the ice of the drainage basin (Rignot and Mouginot, 2012). Observations have shown that the fast flowing areas of Jakobshavn Isbræ exhibit a weak bed with a ~~considerable~~ basal layer of temperate, soft ice (Lüthi et al., 2002). ~~Most of these areas' horizontal motion is due to basal~~ Basal sliding and shear in this layer cause most of these areas' horizontal motion. A large fraction of the ice stream's momentum ~~has to be~~ is transferred to the adjacent ice sheet by lateral stress. It is thus well justified to use the two-dimensional shelfy-stream approximation (SSA, MacAyeal, 1989) ~~for model simulations of~~ to simulate this glacier.

~~The basal topography of Jakobshavn Isbræ and its velocity field permit to roughly~~ We partition the catchment area into the confined, deep and fast-flowing ~~troughs~~ trough ("ice stream") and the surrounding ~~parts of low velocity flow~~ slow-moving ice ("ice sheet"). Those areas are separated by pronounced shear margins ~~to~~ on either side of the ice stream.

[Figure 2 about here.]

Until the late 1990s, ~~the glacier~~ Jakobshavn Isbræ had a substantial floating ice tongue, which extended well into the ~~ice~~ fjord, and was fed by both ~~tributaries. The position of the ice front~~ branches. The calving front position remained fairly constant ~~over time since the 1960s~~from 1962 to the 1990s (Sohn et al., 1998), and the glacier exhibited negligible seasonal variations in flow speed (Echelmeyer and Harrison, 1990). ~~The glacier started an ongoing~~ In the 1990s, the glacier started a phase of acceleration, thinning and retreat, that followed the breakup of its ice tongue. Seasonal variations in ~~ice~~ calving front position and flow velocity increased sharply (Joughin et al., 2004, 2008). ~~The glacier is currently far from equilibrium, making it~~ Today, the glacier is one of the fastest ice streams in the world~~and~~.

It is still far from equilibrium and is a major contributor to global sea level rise (Howat et al., 2011; Joughin et al., 2014). Observations ~~confirm that the current ice stream dynamics are mainly controlled by the position of the ice front~~ suggest that the calving front position is a major control on the ice stream dynamics (Podrasky et al., 2012; Rosenau et al., 2013; Moon et al., 2014).

Various hypotheses have been proposed to explain the mechanisms behind ~~the~~ this change. All identify the breakup of the floating ice tongue as the initial ~~triggering mechanism~~ trigger of this dramatic chain of events, but different ~~possible~~ mechanisms have been proposed to explain the sustained acceleration, thinning and retreat of the glacier. Studies by Joughin et al. (2012) and Habermann et al. (2013) propose loss of buttressing and changes in basal conditions as the main cause behind the ongoing acceleration. On the other hand, van der Veen et al. (2011) argue that ~~the acceleration has to be accompanied by significant~~ weakening of the lateral shear margins has significantly amplified the upstream acceleration. ~~Various~~ Several modelling studies of the glacier, which use 1D-flowline and 2D-flowband models, project unstable retreat of the glacier along its southern trough for up to 60 km inland within the next century (Vieli and Nick, 2011; Joughin et al., 2012; Nick et al., 2013). Other modelling studies argue that this type of ice stream ~~displays stable behaviour~~ is stable as long as it is ~~being~~ fed by the surrounding ice sheet (Truffer and Echelmeyer, 2003). However, numerical 2D planview modelling efforts of Jakobshavn Isbræ ~~in the horizontal plane~~ so far lacked the representation of a dynamically evolving ~~ice~~ calving front. Hence, the hypotheses could not be tested in a satisfactory manner.

We present here a ~~theoretical and technical framework for a LSM used~~ LSM-based framework to model the dynamic evolution of ~~an ice~~ a calving front. This method ~~tracks the ice front related boundary conditions and~~ is a step towards ~~a more~~ better physical representation of ~~ice~~ calving front dynamics in 2D and 3D ice sheet models. We ~~implemented the~~ describe the implementation of the method into the Ice Sheet System Model (ISSM, Larour et al., 2012b), a parallel, ~~state- of-the-art FEM~~ state-of-the-art ice sheet model, and apply it here to Jakobshavn Isbræ in order to model ~~the~~ its dynamic response to perturbations in calving rate~~and conclude on its sensitivity to ice front retreat over the next 120 years~~.

2 Theory

2.1 Ice Flow Model

We employ the SSA on both floating and grounded ice. It neglects all vertical shearing but includes membrane stresses. The ice viscosity, μ, follows Glen's flow law (Glen, 1958):

$$2\mu = B\dot{\varepsilon}_e^{\frac{1-n}{n}} \tag{1}$$

Here, $n = 3$ is Glen's flow law coefficient, B the ice viscosity parameter, and $\dot{\varepsilon}_e$ the effective strain rate. We apply a Neumann stress boundary condition at the ice-air and ice-water interface, corresponding to zero air pressure and hydrostatic water pressure, respectively. A linear friction law links basal shear stress, $\boldsymbol{\sigma}_b$, to basal sliding velocity, $\boldsymbol{v}_b$, on grounded ice:

$$\boldsymbol{\sigma}_b = -\alpha^2 N \boldsymbol{v}_b\,, \tag{2}$$

where α denotes the basal friction parameter. We calculate the effective basal pressure, N, assuming that sea water pressure applies everywhere at the glacier base, which is a crude approximation far from the grounding line. The ice thickness, H ~~evolves~~, evolves over time according to the mass transport equation:

$$\frac{\partial H}{\partial t} = -\nabla \cdot (H\boldsymbol{v}) + a_s + a_b. \tag{3}$$

Here, $\boldsymbol{v}$ is the depth-averaged horizontal ice velocity, and a_s and a_b are the surface and basal mass balance, respectively. We determine the grounding line position using hydrostatic equilibrium, and treat it with a sub-element parametrisation (Seroussi et al., 2014). We refer the reader to ~~Greve and Blatter (2009), Cuffey and Paterson (2010) and Larour et al. (2012b) respectively, for further details on ice flow modelling and its implementation~~ Larour et al. (2012b) for details on the solution of these equations in ISSM.

[Table 1 about here.]

2.2 Level-Set Method

Let Ω be a computational domain in ~~two- or three-dimensional~~ 2D or 3D space, and φ a real, differentiable function on ~~$\Omega \times [0,\infty)$.~~ $\Omega \times \mathbb{R}_+$, called "Level-Set Function" (LSF). For any $c \in \mathbb{R}$, we define the contour, or "c-level-set", of φ by $\varphi(\boldsymbol{x},t) = c$. Taking its material derivative yields the "Level-Set Equation" (LSE):

$$\frac{\partial \varphi}{\partial t} + \boldsymbol{w} \cdot \nabla \varphi = 0. \tag{4}$$

This Hamilton-Jacobi type partial differential equation describes how level-sets move with the local value of the velocity $\boldsymbol{w}$, which is called level-set velocity. We need to provide an initial condition $\varphi_0(\boldsymbol{x}) = \varphi(\boldsymbol{x}, t=0)$ to solve eq. (4).

We use φ to partition Ω ~~at time t~~ into three disjoint subdomains: the ice domain, $\Omega_\mathrm{i}(t)$, its complement, $\Omega_\mathrm{c}(t)$, and their common boundary, $\Gamma(t)$~~.~~:

$$\begin{cases} \varphi(\boldsymbol{x},t) < 0 \Leftrightarrow \boldsymbol{x} \in \Omega_\mathrm{i}(t) \\ \varphi(\boldsymbol{x},t) = 0 \Leftrightarrow \boldsymbol{x} \in \Gamma(t) \\ \varphi(\boldsymbol{x},t) > 0 \Leftrightarrow \boldsymbol{x} \in \Omega_\mathrm{c}(t) \end{cases}$$

We omit the time dependence of these sets in the ~~following, unless stated otherwise. Let $\boldsymbol{x}$ be a point in Ω. If $\varphi(\boldsymbol{x},t) < 0$, then $\boldsymbol{x}$ belongs to Ω_i. If $\varphi(\boldsymbol{x},t) = 0$, then $\boldsymbol{x}$ lies on Γ. If $\varphi(\boldsymbol{x},t) > 0$, then $\boldsymbol{x}$ belongs to Ω_c.~~ remainder of this article. By construction, Γ, the ~~0-contour or "~~0-level-set ~~"~~ of φ, separates Ω_i and Ω_c.

~~A particle at the boundary Γ moves with the boundary speed $\boldsymbol{w}$. This motivates the "Level-Set Equation" (LSE):~~

$$\cancel{\frac{\partial \varphi}{\partial t} + \boldsymbol{w} \cdot \nabla \varphi = 0.}$$

~~This Hamilton-Jacobi type partial differential equation describes the transport of the ice boundary across Ω. We need to provide an initial field $\varphi_0(\boldsymbol{x}) = \varphi(\boldsymbol{x}, t=0)$ on Ω to solve equation (4). We can propagate the unit surface normal~~ We extend $\boldsymbol{n}$~~on~~, the outward-pointing unit normal of Γ, onto Ω using the LSF by:

$$\boldsymbol{n} = \frac{\nabla \varphi}{|\nabla \varphi|}. \tag{5}$$

~~By definition, $\boldsymbol{n}$ always points into Ω_c. For more~~ For details on the Level-Set Method and its applications, we refer to Osher and Sethian (1988) and Sethian (2001).

[Figure 3 about here.]

The boundary position of an ice sheet evolves with ~~a velocity, which is~~ the sum of the ice velocity $\boldsymbol{v}$ and an ablation velocity $\boldsymbol{a} = -a^{\perp}\boldsymbol{n}$. The ablation rate~~$a^{\perp} = -\boldsymbol{a} \cdot \boldsymbol{n}$~~, $a^{\perp}$, is ~~non-negative in compliance with current glaciology terminology, and is~~ the difference between ~~ice boundary velocity $\boldsymbol{w}$~~ the level-set velocity and ice velocity ~~$\boldsymbol{v}$~~ projected along $\boldsymbol{n}$:

$$a^{\perp} = (\boldsymbol{v} - \boldsymbol{w}) \cdot \boldsymbol{n}. \tag{6}$$

It follows that the ice boundary is stationary ($\boldsymbol{w} \cdot \boldsymbol{n} = 0$) if and only if $a^{\perp} = \boldsymbol{v} \cdot \boldsymbol{n}$, i.e. the ablation rate matches the ice velocity perpendicular to the ice boundary. The ablation rate ~~$a^{\perp}$ can be an input taken from observations or a suitable~~ needs to be prescribed, either based on observations or through a parametrisation.

Note that no limitations have been made so far with respect to the dimension of the problem in this section. Accordingly, the method could be applied to model the evolution of the glacier thickness and lateral extent simultaneously (Pralong and Funk, 2004). However, here we use the LSM to model only the horizontal extent of the ice sheet. Its vertical extent is described by the mass transport equation (3). ~~We~~ ISSM relies on vertically extruded meshes and the vertical motion of the ice boundary is accurately captured by redistributing the horizontal layers of the mesh. Using the LSM in the vertical dimension would not only significantly complicate its implementation, but it would also reduce the accuracy and precision of the ice boundary tracking (see also section 2.3).

For simplicity, we assume in the remainder of the article that lateral ablation occurs in the form of calving, with a calving velocity $\boldsymbol{c} = -c^{\perp}\boldsymbol{n}$~~, and that calving itself is~~. Calving itself is assumed to be a quasi-continuous process, consisting of frequent, but small calving events. With (5) and (6), equation (4) becomes:

$$\frac{\partial \varphi}{\partial t} + \boldsymbol{v} \cdot \nabla \varphi = c^{\perp} |\nabla \varphi|, \tag{7}$$

which is also known as "Kinematic Calving Front Condition" (KCFC, Greve and Blatter, 2009). ~~The calving rate needs~~ Both the calving rate and ice velocity need to be provided ~~as a~~ on the entire 2D ~~field on~~ computational domain Ω ~~, that can also vary with time~~in order to solve the KCFC. An example of a calving rate field ~~can be seen in~~ will be given in section 3.2, and is shown in Fig. 4. The ~~ice~~ KCFC implies that all level-sets of φ, including the calving front Γ~~is advected at any~~, move at a given time with the local sum of the horizontal ice velocity and ~~local calving rate values at the current ice front position~~ calving rate along the normal $\boldsymbol{n}$ (Fig. 3). We define the ~~"calving flux " to be the ice volume calving at the ice frontper unit time~~calving flux Q_{cf} as the ice flux crossing the calving front:

$$Q_{\mathsf{cf}} = \int_{\Gamma} c^{\perp}(r) H(r)\, dr. \tag{8}$$

~~Calving rate and velocity need to be given on the entire computational domain Ω in order to solve the KCFC. Since field variableslike velocity and thickness are only available~~ Some variables, like the ice velocity, are only defined on Ω_i, ~~we need to propagate them continuously~~ and need to be extended onto Ω_c. ~~We extrapolate such a fieldvariable~~ Any scalar field, S, is extrapolated onto Ω_c by solving:

$$\boldsymbol{n} \cdot \nabla S = 0, \tag{9}$$

while keeping ~~it~~ S fixed on Ω_i. This type of extrapolation has the tendency to preserve $|\nabla \varphi| = \mathcal{O}(1)$, when we use the extrapolated ice velocity field to solve the KCFC (Zhao et al., 1996).

2.3 Implementation

ISSM relies on the ~~FEM~~ Finite Element Method (FEM) to solve partial differential equations. It applies a Continuous Galerkin FEM using triangular (2D) and prismatic (3D) Lagrange finite elements, and uses anisotropic mesh refinement to limit the number of degrees of freedom while maximizing spatial resolution in regions of interest.

We discretise the KCFC (7) and extrapolation equation (9) using linear finite elements on the same mesh as the one used to model the ice dynamics. We stabilise both equations with artificial diffusion (Donea and Huerta, 2003), which after thorough testing proved to be the most robust stabilisation scheme. We integrate over time using a semi-implicit ~~finite difference~~ time-stepping scheme. We solve the KCFC~~(7)~~, and the field equations for ice flow modelling in a decoupled fashion. The KCFC is solved first with input data from the ~~last~~ previous time step. We then update the numerical ice domain ~~$\Omega_\mathrm{i}^\mathrm{h}$~~ using the new LSF as described below, and update boundary conditions accordingly. ~~We finally~~ Finally, we solve the momentum balance and the mass transport equation on ~~Ω_i~~ the updated ice domain.

The 0-level-set of φ, Γ, does in general not coincide with the finite element mesh edges due to its implicit representation. ~~The ice front Γ~~ It intersects a number of elements ("front elements") with a hyperplane, which divides them into an ice-filled and an ice-free ~~domain~~ part (Fig. 3). ~~Ice velocity and ice thickness exhibit a discontinuity at subgrid scale here,~~

~~which we cannot resolve using the Continuous Galerkin FEM.~~ This has various implications on the numerical level. When assembling the system stiffness matrices for ice flow modelling, exclusive integration over the ice-filled part of the element would be required. The stress boundary condition at the ~~ice~~ calving front would have to be applied at the intersecting hyperplane. Currently, ISSM is not capable of resolving those submesh scale processes.

Therefore, we ~~opt to~~ either fully activate or deactivate ~~an~~ a mesh element at every time step. Only active elements are considered for the numerical discretisation of the respective field equations. We activate ~~a mesh~~ an element if at least one of its vertices is in Ω_i or Γ~~.~~ ~~Then we consider the entire element to consist of~~ , and the element is then considered to be entirely filled with ice. We flag the element as ice free if it lies entirely inside Ω_c, and it is deactivated~~at this time step~~. As a consequence, the numerical ~~ice front~~calving front, Γ^h, runs along mesh edges, and ~~updates of Γ^h occur~~ is updated in a discontinuous manner ~~.~~ (Fig. 3). We apply the stress boundary condition along Γ^h for numerical consistency. ~~The strongly viscous ice rheology efficiently dampens effects of these discrete boundary condition updates.~~ ~~Ice~~ Calving front normals on Γ and Γ^h may differ significantly in direction. However, stress components tangential to $\boldsymbol{n}$ cancel out along Γ^h, so that the integrated stress exerted at the ~~ice~~ calving front is close to the one applied along Γ. For all further calculations where a normal is involved, like extrapolation, the normal to the LSF (5) is used.

The ~~ice domain Ω_i~~ numerical calving front is by definition ~~a subset of the numerical ice domain $\Omega_\mathrm{i}^\mathrm{h}$. Γ^h is thus displaced~~ further downstream than Γ. This may lead to slightly higher resistive lateral stress at the ~~ice~~ calving front, whose magnitude depends on the excess ice area of the intersected front element and the front geometry. We ~~choose~~ use a fine mesh resolution in the vicinity of the ~~ice~~ calving front to limit this effect.

We extrapolate the ~~ice~~ calving front thickness onto the ice-free ~~vertices of the front elements~~ domain using equation (9). This yields realistic ice thickness and ice thickness gradients across the front elements, that would otherwise lead to overestimated driving stress and underestimated water pressure at the ice-ocean interface. If not corrected, those two effects unrealistically increase ice velocities at the ~~ice~~ calving front, which then feed back into the mass transport and LSM schemes.

We present ~~an idealized test-setup~~ two experiments for validation of the ~~LSM-module in Appendix A. It~~ LSM implemented here in the Appendix. The first experiment shows that the ice margin is advected with ~~correct speed. A small error is due to the underlying unstructured mesh used, but~~ the prescribed level-set velocity $\boldsymbol{w}$. The linear representation of the LSF on an unstructured mesh causes a small error in the exact level-set position, which depends on element size and cancels out over time. The ~~module~~ second test shows that errors in volume conservation introduced by the LSM decrease with finer mesh resolution, and are below 0.2 % after 100 years for a mesh resolution of 1 km. In the application to Jakobshavn Isbræ, we use a front element size of 0.5 km. The potential volume loss inherent to this implementation of the LSM is thus far below current uncertainties of model input data.

Inclusion of the LSM requires additional computational effort for the extrapolation of field variables, to solve the KCFC, and for extra iterations of the momentum balance solver, since the stress boundary ~~condition at the ice front does often change~~ conditions at the calving front change frequently. Its amount depends on the flow approximation ~~used~~ and especially on whether the model setup is close to a stable configuration or not. Using ~~the SSAapproximation~~SSA, the additional computational cost ~~amounts to~~ reaches up to 25%, of which 11% is caused by the solution of the ~~LSM-module for this experiment~~KCFC.

3 Data and model setup

3.1 Jakobshavn Isbræ Model Setup

We use Jakobshavn Isbræ's drainage basin from Zwally et al. (2011) to generate a 2D-horizontal finite element mesh with element size varying from 500 m in the fjord and areas of fast flow to 10 km inland (Fig. 4). We choose this high mesh resolution to minimise ~~ice~~ calving front discretisation errors, and to resolve the fjord and the deep trough accurately in the model. The resulting mesh has about 10,000 vertices and 19,000 elements. Due to high flow velocities, the ~~numerical~~ Courant-Friedrich-Lewy condition ~~(Courant et al., 1928)~~ (CFL, Coura a time step ~~length~~ on the order of days.

We use ~~ice bedrock~~ bed topography from Morlighem et al. (2014), derived using a mass conservation approach (Morlighem et al., 2011). The ice surface elevation is taken from GIMP (Howat et al., 2014)~~. Ice~~ , and ice thickness is the difference between ice surface and ice base elevation. Bathymetry of the ice-choked fjord of Jakobshavn Isbræ is difficult to measure and currently poorly known. As a first order estimate, we apply a parabolic profile of 800 m depth along the ice fjord, fitted via spline interpolation to known topography data. We rely on Ettema et al. (2009) ~~to force~~ for the surface mass balance. Their surface temperatures are used to calculate the ice viscosity parameter, B, following an Arrhenius relationship (Cuffey and Paterson, 2010) ~~once~~ at the beginning of the model simulations. Basal mass balance is set to zero and no thermal model is run. All these forcings are kept constant over time.

We infer a basal friction coefficient, α, in (2) using an adjoint-based inversion (MacAyeal, 1993; Morlighem et al., 2010) of ~~existing InSAR-derived~~ surface velocities from 2009 (Rignot and Mouginot, 2012). In regions like the ~~ice~~ fjord, where there is no ice today, we apply an ~~averaged~~ area-averaged value of $\alpha = 30$ a$^{1/2}$m$^{-1/2}$. At the margins of the computational domain we prescribe zero horizontal ice velocities in order to prevent mass flux across this boundary. ~~α~~ The friction parameter is kept fixed over time for all model simulations.

Inconsistencies in model input data cause sharp readjustments of the glacier state at the beginning of each simulation, which would make it difficult to distinguish between such effects and those of the applied forcing (Seroussi et al., 2011). Therefore, we relax the ~~ice surface~~ model prior to the experiments using a fixed~~ice front, whose position and orientation is set~~ , piecewise linear LSF φ_0, whose 0-level-set corresponds to the mean annual ~~ice~~ calving front position of ~~2009.~~ 2009 (Fig. 4). Since the glacier in this configuration is far from steady state, model relaxation causes considerable thinning across the glacier's catchment area. In order not to deviate too much from present day's geometric setting we choose a 100 year relaxation time ~~interval~~period. Note that the grounding line retreats during the relaxation due to dynamic thinning, so that the glacier forms a new floating ice tongue. This ice tongue extends about 15 km to a ~~topographic high~~ local topographic maximum in the southern trough and 3 km into the northern one (Fig. 4). The relaxed geometry constitutes the initial state for our experiments.

Due to this deviation in geometry, providing quantitative insights into Jakobshavn Isbræ is beyond the scope of this study. However, the main characteristics of the ice stream (e.g. its large drainage basin and the narrow outlet channel) are preserved, so that the results presented in this paper qualitatively represent the behaviour of Jakobshavn Isbræ.

[Figure 4 about here.]

3.2 Description of experiments

For simplicity, frontal ablation occurs ~~in the experiments~~ exclusively in the form of calving ~~. We let~~ in the experiments. We set

$$c_0^{\perp} = \cancel{l\cdot} q|\boldsymbol{v}_0| \qquad (10)$$

as a basic calving rate estimate, motivated by the small observed angle between $\boldsymbol{v}$ and $\boldsymbol{n}$ at the ~~ice front .~~ calving front ($\boldsymbol{v} \approx |\boldsymbol{v}|\boldsymbol{n}$). Then $\boldsymbol{w}\cdot\boldsymbol{n} = \boldsymbol{v}\cdot\boldsymbol{n} - \boldsymbol{c}\cdot\boldsymbol{n} \approx 0$, so that we can expect this calving rate estimate to yield a stationary calving front, if applied to a geometry that is in steady state. Here, $\boldsymbol{v}_0$ denotes the velocity field at the end of the geometry relaxation run, ~~continued~~ extended onto Ω_{c} (Fig. 4). ~~l is a continuous function , which is~~ The continuous function q is equal to 1 in areas where the ~~bedrock~~ bed lies below -300 m, and linearly drops to 0 in areas of positive ~~bedrock~~ bed elevation. It prevents calving ~~onto~~ to occur in areas with a glacier bed above sea level, ~~motivated by observations from~~ as suggested by observations of tidewater glaciers (Brown et al., 1982). We ~~expect this calving rate to yield a stationary ice front, if applied to a geometry in steady state. We~~ scale $c_0^{\perp}$ over time with a scaling function ~~$s = s(t)$,~~ , s, which allows for the representation of seasonal ~~calving~~ cycles, and a perturbation function ~~$p = p(t)$~~ , p, to modify the calving rate for some period of time~~, respectively~~. The applied calving rate ~~then is $c^{\perp} = c^{\perp}(\boldsymbol{x},t) = c_0^{\perp}(\boldsymbol{x}) \cdot s(t) \cdot p(t)$~~is then: $c^{\perp}(\boldsymbol{x},t) = c_0^{\perp}(\boldsymbol{x})\, s(t)\, p(t)$.

We perform three suites of experiments in order to analyse the impact of the calving rate on the glacier's dynamics. The ~~ice~~ calving front is now allowed to freely evolve in response to $c^{\perp}$. All experiments run for ~~a total time of~~ 120 years.

In experiment A, we keep ~~calving~~ the calving rate constant over time, i.e. we ~~let~~ set both $s(t) = p(t) = 1$. Hence, $c^{\perp}(\boldsymbol{x},t) = c_0^{\perp}(\boldsymbol{x})$. This experiment, although not physically motivated, is used to evaluate whether a stable ~~ice~~ calving front position can be reached using the LSM, and for comparison to the experiments described below.

In experiment suites B and C, we ~~mimic seasonal calving~~ represent the seasonal cycle by scaling $c_0^{\perp}$ ~~over time by a factor~~ by $s(t) = \max(0, \pi \sin(2\pi(t/L - \phi_0)))$, with a phase shift $\phi_0 = 4/12$ and ~~period $L = 1$ a~~a period $L = 1$ a. We perturb the calving ~~cycle~~ rate during a limited ~~perturbation duration~~duration, Δt, with a perturbation strength $p_0 \geq 0$: $p(t) = \begin{cases} p_0, & \text{if } t_0 < t < t_0 + \Delta t, \text{ and} \\ 1, & \text{else.} \end{cases}$

We start the perturbation at $t_0 = 20$ a for all experiments. In experiment suite B~~we choose~~, we perform 5 experiments with $\Delta t = 1$ a~~and vary~~, while varying p_0 ~~in steps of 1~~ from 0 to ~~4. On the other hand, in~~ 4 by increments of 1. In experiment suite C, we keep $p_0 = 2$ fixed, and ~~choose~~ set Δt as 2, 4 and 8 years. We use the notation B<p_0> and C<Δt> to identify ~~the~~ single experiments, e.g. ~~B2~~ B1 for experiment B with perturbation strength ~~$p_0 = 2$. Experiment B1 represents in this experiment suite~~ $p_0 = 1$, which represents the case of unperturbed periodic calving. ~~It~~ B1 is used as a control run the other experiments can be compared to. ~~We introduce $P = (1 - p_0) \cdot \Delta t$, which is a measure of the time-integrated deviation in applied calving rate relative to B1.~~ Table 2 lists all the experiments performed here.

[Table 2 about here.]

4 Results

[Figure 5 about here.]

~~We present ice~~ Fig. 5 shows calving front positions for ~~several experiments in Fig. 5.~~ experiments A, B1, B2 and C4. Under constant calving rate forcing, the ~~ice front essentially~~ calving front remains at a stable position after minor readjustments in the first decade of the simulation. In experiment A, the ~~ice~~ calving front undergoes gradual retreat over time. When we perturb the calving rate, the ~~ice front migrates. Increased calving rates cause ice front retreat:~~ calving front migrates, and higher calving rates lead to larger retreats. The retreat is highest in areas of fast ~~ice flow, but~~ flow, and strongly decreases towards the ice stream margins. This yields the characteristic concave shape of a retreating ~~ice front. Resulting ice fronts~~ calving front. The modelled calving front positions and their ~~characteristics do agree well with ice fronts obtained from~~ shape are in good agreement with observations (Fig. 2). ~~Ice front positions of all~~ The retreat rate during continued phases of calving decreases to zero, so that the calving front reaches a new stable position 9 km upstream of its initial position (Fig. 5d). In experiments B and C ~~readvance after the perturbation interval to a position which is indistinguishable from the one of~~ the calving front returns to a similar position as in the unperturbed experiment B1 ~~in one to two decades~~within ten to twenty years after the perturbation stops.

[Figure 6 about here.]

~~Figure~~ Fig. 6 shows ice velocity, geometry and strain rates ~~along two tracks~~for experiment C4 along two lines, which go along and across the southern trough, respectively (Fig. 4). ~~We observe that the ice front position, its ice velocity and thickness as well as the position of the grounding line form an ensemble, which quickly adjust to each other under constant mean annual calving rates to reach a characteristic “ice front configuration”. The variables of the ice front configuration mirror the minor adjustment of the ice front position~~ During the first 20 years prior to the perturbation~~. Only~~ , the ice thickness in the floating part decreases ~~up to~~ by about 100 metres ~~once the ice front is allowed to freely adjust.~~

(Fig. 6a). ~~Enhanced calving causes the modelled ice stream to rapidly thin, accelerate and retreat. However, the ice front can be very thick at the end of the calving season, as the glacier has retreated back into areas of high ice thickness . Ice velocities respond to this change by increasing over time as the ice front retreats and peaking at the point of furthest retreat. The response is stronger with larger and longer perturbations, as expected.~~ As the calving front retreats during the perturbation, the ice velocity increases (Fig. 6b), and the ice thickness adjusts accordingly (Fig. 6a). The ice thinning leads to a fast retreat of the grounding line in the regions of locally retrograde bed, and temporarily stabilises over local along-trough topographic maxima, referred to as “local highs”. The southern trough has many local highs, which act as pinning points and are critical for flow dynamics, in agreement with earlier results from Vieli and Nick (2011). The acceleration of the ice stream extends ~~well upstream~~tens of kilometres upstream, to areas of grounded ice ~~. Both thinning and acceleration mainly occur in~~ (Fig. 6b). Thinning and acceleration are strongest over the ice stream~~itself, and diffuse~~ , and spread out to the surrounding ice sheet in a ~~strongly~~ dampened fashion. These thinning and acceleration patterns increase surface and velocity gradients~~along and across the ice stream~~, especially in the shear margins ~~. Here, the ice stream acceleration gradually increases~~ (Fig. 6c), where the effective strain rates gradually increase up to a factor of 4 in experiment C4 (Fig. 6d), which corresponds to a drop in viscosity of about 60% (equation 1). This substantially weakens the mechanical coupling between the ice stream and the surrounding ice sheet~~substantially. The grounding line position lies downstream of a local high of the basal topography at any given time of the experiment, even if the general slope of the basal topography is retrograde. It is hardly affected by small calving rate perturbations. However, large perturbations cause discontinuous migration of its position to the next topographic high upstream. Their discrete locations form the set of stable grounding line positions along the deep part of the tributaries. Discontinuous retreat of the grounding line causes drastic, but short-lived flow acceleration, which indicates that the basal topographic highs act as pinning points, even if basal friction coefficient~~ $\cancel{\alpha}$ ~~and effective basal pressure~~ $\cancel{N}$ ~~in the troughs are low.~~ .

[Figure 7 about here.]

~~Timelines of ice front position, ice velocity and thickness at the ice front~~ Fig. 7 shows the intra-annual variability of ice properties at the calving front and grounding line for experiments A, B1, ~~as well as effective strain rate and position of the first grounded point along-trough are shown in Fig. 7. They allow us to study the interannual behaviour of the ice front configuration in more detail.~~ B2 and C4. All shown variables reflect the characteristics of the applied calving rate forcing. ~~They stay constant~~ The constant calving rate applied in experiment A ~~, and oscillate periodically with a constant amplitude around an annual mean value in experiment suites B and C.~~

~~Prior to the perturbation, the ice front position varies~~ leads to a steady configuration (Fig. 7a and 7b). For an unperturbed periodic calving rate forcing (Fig. 7c and 7d), the calving front position oscillates around a constant annual mean value by ±3 km~~along-stream.~~ , while the grounding line position remains unchanged at kilometre 29. Ice velocities and ~~front thickness~~ thickness at the calving front act in phase ~~to the ice~~ with the calving front position, while the response of strain rates at the grounding line is ~~slightly delayed . Ice velocities vary~~ delayed by about a month. The ice velocity varies by ±20%, which corresponds to about ±2 km a^{-1}, the ice thickness by ±13%, or ±100 m, and effective ~~grounding line strain rates~~ strain rates at the grounding line by ±7%, or ±0.1 a^{-1}. ~~The grounding line position is stable at kilometre 29 of the along-trough profile. In~~

The response to a ~~two-fold increase in calving rate , the ice~~ calving rate perturbation scales with p_0 and Δt. When the calving rate doubles (B2, C4), the calving front retreats initially at an average rate of 4.5 km a^{-1}. The calving front stabilizes 9 km upstream for longer perturbations (Fig. 7~~d). This retreat rate decreases to zero for longer perturbations, so that the ice front approaches a new stable position upstream. Variation of the ice front position during the retreat doubles to up to~~ g). The intra-annual variability of the calving front position doubles to ±6.5 km. ~~Average~~ The grounding line position is hardly affected by small calving rate perturbations, but large perturbations trigger fast retreats of several kilometres, which in turn cause drastic, but short-lived flow accelerations (Figs. 7g and 7h). The annual average ice velocity increases by ~~about~~ 10%, ~~but its variation also almost~~ and its intra-annual variability doubles to ±38% ~~. Occasional velocity spikes occur related to~~

~~ungrounding from pinning points. The ice front thins on average by a third, with oscillations~~ (Fig. 7h). The mean calving front thickness decreases by 30% towards the end of the perturbation of experiment C4, and experiences large variations up to ±75%. This high thickness ~~variation~~ variability is due to the ~~calving back~~ front retreating into areas of thick ice in summer followed by stretching and thinning during ~~ice~~ calving front advance in ~~the late winterseason. Variation of the grounding line position remains small during the perturbation, disrupted only by its discontinuous retreat for large perturbations.~~ winter. For small perturbations~~(Fig. 7c), variation~~ , variations of effective strain rates ~~here quadruples~~ at the grounding line quadruple to ±25% ~~.~~ (Fig. 7f). Once the calving rate perturbation ~~ceases, the ice front configuration displays a striking reversibility in all its variables.~~ stops, all variables display remarkable reversibility.

When calving is temporarily turned off (experiment B0, not shown here), the response of the glacier is reversed: the calving front advances, creating a convex ice tongue. Meanwhile, the ice stream decelerates, thickens, and the grounding line advances. After the perturbation, the glacier retreats into a state slightly thicker and faster than the one of experiment B1.

[Figure 8 about here.]

~~Finally,~~ Fig. 8a shows the evolution of the ~~total ice volume as modelled against control runB1. The mean annual volume change due to~~ ice volume with respect to experiment B1, the control run. The glacier in experiment B1 continues to lose volume at an average rate of -22.8 km^{3}a^{-1} due to the ongoing geometry relaxation~~of experiment B1 is -22.8 km^{3}a^{-1}, varying by 10.5 km^3 per year. Experiment Aundercuts this value by -0.4 km^{3}a^{-1} on average related~~ . In experiment A, Jakobshavn Isbræ loses an additional 0.4 km^{3}a^{-1}, which corresponds to the gradual retreat of ~~its ice~~ the calving front. Enhanced calving causes additional volume loss proportional to ~~perturbation measure P. It amounts to -35.7 km^{3}a^{-1}~~ $\Delta t(1-p_0)$, the measure of the time-integrated calving rate perturbation (Fig. 8b). If the calving rate is doubled, the additional volume loss reaches 35.7 km^{3}a^{-1} in the first year~~of perturbation of experiment C8~~, but decreases with time, as the ~~ice~~ calving front thins and retreats into areas of lower calving rates. Those numbers agree well with recent ice discharge observations (Howat et al., 2011). ~~After the~~ Over the first decade after the perturbation, all modelled glaciers recover ~~40-60~~ 40 to 60% of the volume ~~difference in the first decade, because during the readvance the thin ice front strongly reduces the calving flux. The calving flux converges to the value of experiment B1 once the ice front configuration approaches the state of the~~ deviation to the control run. ~~The ice volume now has to be replenished by excess surface accumulation, which takes longer than the 120 years of simulation time presented here. Calving rate perturbations therefore leave a lasting imprint on the ice sheet.~~

~~Results of experiments of decreased calving are not shown here. They exhibit the exact inverse pattern to the one described above for enhanced calving : the ice front advances during the perturbation, creating a convex ice tongue. Meanwhile, the ice streamdecelerates and thickens, causing grounding line advance and volume increase. After the perturbation period, the glacier calves back into a state slightly thicker and faster than the one of B1.~~

5 Discussion

~~The characteristics of the applied calving rate determine the behaviour of~~ The applied calving rate determines the behaviour of the ~~ice front . The ice front will reach a stable configuration if~~ calving front and the ice stream. In our simulations, larger perturbation strengths p_0 lead to faster calving front retreats. In the case of long perturbations (experiments C4 and C8), the calving front reaches a new stable position. A stable calving front position requires the calving rate ~~exceeds~~ to be larger than the ice velocity ~~from some point along-stream onward. It will either retreat back or advance to this point. If no such point exists,~~ if the calving front advances, and similarly, if the calving front retreats, the ~~ice front will undergo either unconfined advance or retreat, depending on the magnitude of the calving rate .~~ calving rate needs to be lower than the ice velocity.

~~Adjustments of the ice front configuration to the current calving rate change the local driving stress, which lead to corresponding changes in thickness and surface gradient, and vice versa. The mass transport mechanism allows the thickness change to diffuse~~

~~upstream. In case of ice front thinning and surface steepening, the increased driving stressleads to enhanced mass flux, causing further upstream thinning , steepening and acceleration.~~

~~We observe multiple secondary feedback mechanisms in addition to the mass transport mechanism, that determine the way the ice sheet adjusts to calving rate forcings.~~ Several mechanisms determine how the model responds to the calving rate forcing. First, a calving rate increase leads to a retreat of the calving front position, ice stream acceleration and dynamic thinning in the vicinity of the terminus. Second, this dynamic thinning increases surface slopes and therefore the driving stress. As the glacier locally speeds up, the ice thinning propagates upstream. The ice stream thins much faster than the surrounding ice sheet, which steepens the surface across the shear margins. Lateral inflow of ice into the ice stream hence increases until it balances the calving flux. This limits the thinning of the ice stream. Thinning of the ice stream ~~leads to reduced basal effective pressure and~~ in turn leads to grounding line retreat and reduction in basal effective pressure, which both reduce basal drag significantly ~~. Detachment of the base from pinning points~~ in the vicinity of the grounding line. We showed that grounding line retreat leads to short-lived, but drastic increases in ice flux. ~~These mechanisms are~~ This mechanism is qualitatively the same as the ~~ones~~ one described in Vieli and Nick (2011) and Joughin et al. (2012).

~~The ice front lengthens during its retreat, which increases the total driving stress exerted by the ice front. Side arms of the main tributaries are now calving directly into the fjord. This increases calving flux~~ $\cancel{Q_{\mathsf{cf}}}$~~, which additionally thins and steepens areas in the immediate ice front vicinity~~Several pinning points along the retrograde trough of the southern branch, as well as the lateral stress transfer and mass influx prevent the modelled ice stream from being prone to the Marine Ice Sheet Instability (Weertman, 1974; Schoof, 2007), a hypothesis which states that grounding line positions are unstable on retrograde slopes. This corroborates earlier results by Gudmundsson et al. (2012), who presented examples of stable grounding line positions on retrograde beds. However, due to large uncertainties in the input data, and since some physical processes are not represented in our experiments, evaluation of this question for Jakobshavn Isbræ is beyond the scope of this study.

~~The steepening of the surface slopes across the shear margins caused by ice stream thinning results in increased driving stress, which increases lateral ice inflow into the ice stream. This in turn limits surface steepening and grounding line retreat along the trough. The feedbacks described above cause a net rise in volume flux towards the ice front and enable quick adjustment of the glacier in response to changes of the ice front configuration~~A third mechanism is related to the calving front lengthening during its retreat (e.g. figure 5). The lengthening causes tributaries of the main ice stream to calve directly into the fjord, thereby increasing the calving flux Q_{cf} (equation 8) and thinning of the terminus vicinity.

~~Acceleration of~~ Finally, the ice stream ~~and surface steepening in its vicinity strongly increase~~ accelerates faster than the surrounding ice sheet, which increases strain rates at the shear margins~~and the grounding line. The non-linear rheology of ice softens~~. This reduces the ice viscosity in these areas, which mechanically decouples the ice stream from the ice sheet, allowing the ice stream to accelerate further~~, and to soften its shear margins more and more~~. This positive feedback ~~is only~~ confines the initial thinning to the ice stream, and is controlled by the rate at which ice ~~is able to enter~~ enters the ice stream~~to sustain the driving stress. We consider this mechanism to be substantial for sustaining the longer term~~. This mechanism is essential for enabling ice stream acceleration tens of kilometres upstream of the grounding line, since large fractions of the ice stream's driving stress ~~is~~ are balanced by lateral stress. This corroborates force balance arguments produced earlier by van der Veen et al. (2011).

~~Reduced lateral momentum transfer decreases lateral mass influx. This makes the surrounding ice sheet less sensitive to short periods of enhanced calving. For this reason, calving induced thinning mainly occurs in the ice stream, which limits the rateat which additional ice can be discharged.~~

~~Conversely, in case of no seasonal calving cycle of experiment A,~~ In experiments A and B1, we apply the same annual mean calving rate. However, due to the lack of seasonal cycle in calving rate the mechanical coupling between the ice stream and ice sheet is higher ~~than compared to experiment B1. Ice~~ in experiment A. The ice stream velocity is therefore lower, ~~which causes net ice~~ causing gradual calving front retreat and ~~corresponding~~ additional ice volume loss. This illustrates that ~~ice sheet models which do not include a seasonal calving cycle may overestimate mass loss of glaciers. Moreover, we do advise against the use of ice models, which do not incorporate~~ volume change estimates from models with and without seasonal cycles of calving may differ. Our results suggest that including both a dynamically evolving ~~ice front nor the related lateral effects, for~~ calving front as well as seasonal cycles are critical for accurate projections of future contributions of ice sheets to global sea level rise on decadal to centennial time scales.

Response mechanisms not covered here will likely include feedbacks ~~in~~ with damage mechanics and thermodynamics due to the increased strain rates. During longer perturbations, ice surface lowering will probably affect the surface mass balance and the drainage basin outline.

The reversibility of the ~~ice~~ calving front configuration after the calving rate perturbation is a robust feature across all experiments. ~~We see the~~ The short duration of the perturbation, the prescribed calving rates~~and the geometric setting of the ice stream to be~~ , and the geometry of the glacier are responsible for this behaviour. ~~Volume change relative to experiment B1 is mainly due to the migration of the ice front and the according change in lateral ice sheet extent. However, the additional ice discharge~~ The volume change in all experiments never exceeds 0.1% of the ~~total~~ initial glacier volume in the experiments shown here. ~~This volume loss can be easily balanced by the vast~~ Once the perturbation stops, the surrounding ice sheet ~~. Since calving rates are not coupled to ice dynamics, the ice front configuration is able to quickly recover once this forcing is set back to its initial value~~continues to replenish the ice stream, which allows for its quick recovery.

The modelled glacier response ~~due~~ to enhanced calving is in good qualitative agreement with observations~~.~~ , which corroborates that calving is a major control on this glacier. The similar shape of the modelled and observed calving front suggests that calving rates are indeed proportional to its flow speed during the glacier's current retreat. However, the reversibility of the ~~ice~~ modelled calving front position is in ~~stark~~ contrast to Jakobshavn Isbræ's ~~ongoing observed retreat. Therefore, the actual calving rates must have stayed increased~~actual behaviour. Sustained high calving rates are therefore necessary to explain the continued retreat of the glacier, as our results suggest that the glacier would have readvanced otherwise. Accurate model input data, representation of all relevant physical processes and incorporation of a suitable calving rate parametrisation will be necessary for quantitative analysis of this dynamic ice stream.

6 Conclusions

~~We presented~~ In this study, we present the theoretical framework for coupling a ~~LSM~~ Level-Set Method (LSM) to ice dynamics and ~~implemented it into the~~ implement it into ISSM. The LSM ~~proved~~ proves to be a robust method for modelling the dynamic evolution of ~~an ice frontsubject to ablation. We applied the~~ a calving front. We apply this technique to Jakobshavn Isbræ using prescribed calving rates~~. We find its dynamics to be~~ , and we find that the glacier is highly sensitive to ~~the applied calving rate~~this forcing, which agrees well with observations.

~~The calving rate perturbation strongly affects the ice flow inland through various mechanisms. Changes~~ Calving rate perturbations strongly affect the ice stream through several linked mechanisms. First, changes in calving rate cause ~~ice~~ calving front migration and alter ~~its~~ the ice discharge. ~~The~~ Second, the resulting thickness change at the ~~ice front diffuses upstream through a coupling between the stress balance and mass transport mechanism. Ice stream thinning reduces basal drag by means of~~ calving front spreads out to the surrounding ice sheet. Third, thinning-induced grounding line retreat ~~and reduction of effective basal pressure. Rheological~~ causes further ice stream acceleration and creates a positive feedback. Finally, shear margin weakening caused by the ice stream acceleration decreases lateral drag ~~resistive to flow. These two positive feedback mechanisms are able to sustain prolonged~~ resisting ice flow. This positive feedback mechanism sustains significant acceleration of the ice stream ~~, and are only controlled by the rate at which ice can enter the ice stream. However, the vast~~ tens of kilometres upstream of the grounding line.

The surrounding ice sheet is barely affected by short periods of enhanced calving. It stabilises the ice stream and allows for quick reversibility of the ~~ice front configuration through~~

~~lateral mass~~ calving front position through lateral ice influx and stress transfer once ~~we set~~ the calving rates are set back to their initial ~~value. The importance of the ice~~ values.

Since the calving front position and ~~lateral effects for~~ dynamic lateral effects are critical to simulate and understand the behaviour of ~~this type of glacier lets us advise against the use of models, which do not represent these mechanisms, for projections of future ice discharge.~~

~~The method presented here is able to close a major gap present in ISSM and various other~~ marine terminating glaciers, the inclusion of moving boundaries in planview and 3D models is key for realistic sea level rise projections on centennial time scales. This method is a step towards better physical representation of calving front dynamics in ice sheet models. ~~It enables a multitude of future studies in combination with e.g. thermodynamics and damage mechanics, and will improve our understanding of outlet glaciers.~~

Appendix A: ~~Test-Setup~~

Appendix: Validation of the Level-Set Method

We present ~~a simple test setup~~ two simple test setups to validate the LSM. The first is designed to show the accurate advection and shape preservation properties of the method. The second setup aims to give an estimate for the volume change introduced by the LSM for different mesh resolutions.

1 Advection

Let Ω be a 50 km square with ~~an~~ the initial LSF as:

$$\varphi_0(\boldsymbol{x}) = \|\boldsymbol{x} - \boldsymbol{x}_0\|_2 - R,$$

where $\boldsymbol{x}_0 = (25, 25)$ km and $R = 12.5$ km, so that ~~our~~ the initial 0-level-set describes a circle in the middle of the domain. We prescribe a constant velocity ~~of~~ ~~$\boldsymbol{v} = 1$ km a$^{-1} \cdot (\cos(\pi/4), \sin(\pi/4))$~~

$\boldsymbol{v} = (\cos(\pi/4), \sin(\pi/4))$ km a^{-1} everywhere. We advect φ_0 over 10 years with time steps of 0.1 a, and keep track of ~~its~~ the 0-level-set.

[Figure 9 about here.]

~~We plot~~ Fig. 9 shows the 0-level-set position at the beginning ~~every year in Fig. 9. The~~ of every year. The LSM preserves the initial circular shape~~is preserved and advected with constant speed~~, and can be used to model both advance and retreat of a calving front.

[Figure 10 about here.]

We measure the advection speed of the 0-level-set along the diagonal marked in white in Fig. 9. Fig. 10 shows the standard deviation of ~~its~~ the numerical error relative to the prescribed advection speed taken over time for different element sizes. The numerical error is ~~mainly related to the interpolated representation~~ due to the linear interpolation of the curved shape~~on an irregular mesh. This causes~~ , which causes variations of the level-set velocity around the ~~front velocity to vary around the mean value, which indeed equals the prescribed velocity~~prescribed value. The standard deviation of the error linearly decreases with mesh ~~width~~resolution, and drops below 1% for elements sizes below 0.5 km. We therefore recommend using ~~an element size of~~ a mesh resolution below 1 km in the ~~ice~~ calving front vicinity for ice sheet simulations.

2 Volume conservation

Let Ω be a 200×20 km^2 rectangle with an initial LSF given by:

$$\varphi_0(\boldsymbol{x}) = (1,0)\cdot\boldsymbol{x} - 100\,\mathrm{km}.$$

The initial lateral extent is thus a 100×20 km^2 rectangle. The geometry corresponds to the Ice Shelf Ramp presented in Greve and Blatter (2009). The ice thickness linearly decreases from 400 m at the grounding line ($x = 0$ km) to 200 m at the calving front ($x = 100$ km). We apply zero surface accumulation and basal melt, as well as zero grounding line velocity and free slip boundary conditions at $y = 0$ km and $y = 20$ km. The ice sheet spreads under its own weight for 100 years. Fig. 11 shows the evolution of the ice volume for different element sizes. All simulations show volume loss due to the free flux boundary condition at the numerical ice front, which is not entirely balanced by the volume added through the ice thickness extrapolation. The volume loss decreases with element size, and is below 0.2% of the initial ice volume after 100 years for an element size of 1 km. This volume loss is far below current uncertainties of other model input data.

[Figure 11 about here.]

Acknowledgements. A. Humbert acknowledges support of the DLR proposal HYD2059 which provides TerraSAR-X data for the project HGF-Alliance Remote Sensing and Earth System Dynamics. The authors thank G. Jouvet and J. Bassis for their helpful and insightful comments.

References

Benn, D. I., Warren, C. R., and Mottram, R. H.: Calving processes and the dynamics of calving glaciers, Earth-Science Reviews, 82, 143–179, doi:10.1016/j.earscirev.2007.02.002, 2007.

Brown, C., Meier, M., and Post, A.: Calving speed of Alaska tidewater Glaciers, with application to Columbia Glacier, Alaska, U.S. Geological Survey Professional Paper, pp. 1258–C., 1982.

Chang, Y.-C., Hou, T., Merriman, B., and Osher, S.: A level set formulation of Eulerian interface capturing methods for incompressible fluid flows, Journal of computational Physics, 124, 449–464, 1996.

Courant, R., Friedrichs, K., and Lewy, H.: Über die Partiellen Differenzengleichungen der Mathematischen Physik, Mathematische Annalen, 100, 32–74, 1928.

Cuffey, K. M. and Paterson, W. S. B.: The Physics of Glaciers, Elsevier, Burlington, Mass., 2010.

Donea, J. and Huerta, A.: Finite Element Methods for Flow Problems, John Wiley & Sons, Chichester, UK, 2003.

Echelmeyer, K. and Harrison, W. D.: Jakobshavns Isbrae, West Greenland: seasonal variations in velocity - or lack thereof, 1990.

Ettema, J., van den Broeke, M. R., van Meijgaard, E., van de Berg, W. J., Bamber, J. L., Box, J. E., and Bales, R. C.: Higher surface mass balance of the Greenland ice sheet revealed by high-resolution climate modeling, Geophysical Research Letters, 36, doi:10.1029/2009GL038110, l12501, 2009.

Glen, J. W.: The flow law of ice: A discussion of the assumptions made in glacier theory, their experimental foundations and consequences, IASH Publ, 47, 171–183, 1958.

Gogineni, S., Yan, J.-B., Paden, J., Leuschen, C., Li, J., Rodriguez-Morales, F., Braaten, D., Purdon, K., Wang, Z., Liu, W., and Gauch, J.: Bed topography of Jakobshavn Isbræ, Greenland, and Byrd Glacier, Antarctica, Journal of Glaciology, 60, 813–833, doi:10.3189/2014JoG14J129, 2014.

Greve, R. and Blatter, H.: Dynamics of ice sheets and glaciers, Springer, Berlin, Germany, 2009.

Groß, S., Reichelt, V., and Reusken, A.: A finite element based level set method for two-phase incompressible flows, Computing and Visualization in Science, 9, 239–257, doi:10.1007/s00791-006-0024-y, 2006.

Gudmundsson, G. H., Krug, J., Durand, G., Favier, L., and Gagliardini, O.: The stability of grounding lines on retrograde slopes, The Cryosphere, 6, 1497–1505, doi:10.5194/tc-6-1497-2012, 2012.

Habermann, M., Truffer, M., and Maxwell, D.: Changing basal conditions during the speed-up of Jakobshavn Isbræ, Greenland, The Cryosphere, 7, 1679–1692, doi:10.5194/tc-7-1679-2013, 2013.

Howat, I. M., Ahn, Y., Joughin, I., van den Broeke, M. R., Lenaerts, J. T. M., and Smith, B.: Mass balance of Greenland's three largest outlet glaciers, 2000-2010, Geophysical Research Letters, 38, doi:10.1029/2011GL047565, 2011.

Howat, I. M., Negrete, A., and Smith, B. E.: The Greenland Ice Mapping Project (GIMP) land classification and surface elevation data sets, The Cryosphere, 8, 1509–1518, doi:10.5194/tc-8-1509-2014, 2014.

Joughin, I., Abdalati, W., and Fahnestock, M.: Large fluctuations in speed on Greenland's Jakobshavn Isbrae glacier., Nature, 432, 608–10, doi:10.1038/nature03130, 2004.

Joughin, I., Howat, I. M., Fahnestock, M., Smith, B., Krabill, W., Alley, R. B., Stern, H., and Truffer, M.: Continued evolution of Jakobshavn Isbrae following its rapid speedup, Journal of Geophysical Research, 113, F04 006, doi:10.1029/2008JF001023, 2008.

Joughin, I., Smith, B. E., Howat, I. M., Floricioiu, D., Alley, R. B., Truffer, M., and Fahnestock, M.: Seasonal to decadal scale variations in the surface velocity of Jakobshavn Isbrae, Greenland: Observation and model-based analysis, Journal of Geophysical Research, 117, F02 030, doi:10.1029/2011JF002110, 2012.

Joughin, I., Smith, B. E., Shean, D. E., and Floricioiu, D.: Brief Communication: Further summer speedup of Jakobshavn Isbræ, The Cryosphere, 8, 209–214, doi:10.5194/tc-8-209-2014, 2014.
Jouvet, G., Picasso, M., Rappaz, J., and Blatter, H.: A new algorithm to simulate the dynamics of a glacier: theory and applications, Journal of Glaciology, 54, 801–811, 2008.
Larour, E., Schiermeier, J., Rignot, E., Seroussi, H., Morlighem, M., and Paden, J.: Sensitivity Analysis of Pine Island Glacier ice flow using ISSM and DAKOTA, Journal of Geophysical Research, 117, F02 009, doi:10.1029/2011JF002146, 2012a.
Larour, E., Seroussi, H., Morlighem, M., and Rignot, E.: Continental scale, high order, high spatial resolution, ice sheet modeling using the Ice Sheet System Model (ISSM), Journal of Geophysical Research, 117, F01 022, doi:10.1029/2011JF002140, 2012b.
Lüthi, M., Funk, M., Iken, A., Gogineni, S., and Truffer, M.: Mechanisms of fast flow in Jakobshavns Isbræ, Greenland, Part III: Measurements of ice deformation, temperature and cross-borehole conductivity in boreholes to the bedrock, Journal of Glaciology, 48, 369–385, 2002.
MacAyeal, D. R.: Large-scale ice flow over a viscous basal sediment: Theory and application to ice stream B, Antarctica, doi:10.1029/JB094iB04p04071, 1989.
MacAyeal, D. R.: A tutorial on the use of control methods in ice sheet modeling, J. Glaciol, 39, 91–98, 1993.
Moon, T., Joughin, I., Smith, B., Broeke, M. R., Berg, W. J., Noël, B., and Usher, M.: Distinct patterns of seasonal Greenland glacier velocity, Geophysical research letters, 41, 7209–7216, 2014.
Morlighem, M., Rignot, E., Seroussi, H., Larour, E., Ben Dhia, H., and Aubry, D.: Spatial patterns of basal drag inferred using control methods from a full-Stokes and simpler models for Pine Island Glacier, West Antarctica, Geophysical Research Letters, 37, doi:10.1029/2010GL043853, l14502, 2010.
Morlighem, M., Rignot, E., Seroussi, H., Larour, E., Ben Dhia, H., and Aubry, D.: A mass conservation approach for mapping glacier ice thickness, Geophysical Research Letters, 38, doi:10.1029/2011GL048659, l19503, 2011.
Morlighem, M., Rignot, E., Mouginot, J., Seroussi, H., and Larour, E.: Deeply incised submarine glacial valleys beneath the Greenland ice sheet, Nature Geoscience, 7, 418–422, doi:10.1038/ngeo2167, 2014.
Nick, F. M., Vieli, A., Howat, I. M., and Joughin, I.: Large-scale changes in Greenland outlet glacier dynamics triggered at the terminus, Nature Geoscience, 2, 110–114, doi:10.1038/ngeo394, 2009.

Nick, F. M., Vieli, A., Andersen, M. L., Joughin, I., Payne, A., Edwards, T. L., Pattyn, F., and van de Wal, R. S. W.: Future sea-level rise from Greenland's main outlet glaciers in a warming climate., Nature, 497, 235–8, doi:10.1038/nature12068, 2013.

Osher, S. and Sethian, J. a.: Fronts propagating with curvature-dependent speed: Algorithms based on Hamilton-Jacobi formulations, Journal of Computational Physics, 79, 12–49, doi:10.1016/0021-9991(88)90002-2, 1988.

Podrasky, D., Truffer, M., Fahnestock, M., Amundson, J. M., Cassotto, R., and Joughin, I.: Outlet glacier response to forcing over hourly to interannual timescales, Jakobshavn Isbræ, Greenland, Journal of Glaciology, 58, 1212–1226, doi:10.3189/2012JoG12J065, 2012.

Pralong, A. and Funk, M.: A level-set method for modeling the evolution of glacier geometry, Journal of Glaciology, 50, 485–491, doi:10.3189/172756504781829774, 2004.

Rignot, E. and Mouginot, J.: Ice flow in Greenland for the International Polar Year 2008-2009, Geophysical Research Letters, 39, 1–7, doi:10.1029/2012GL051634, 2012.

Rignot, E., Jacobs, S., Mouginot, J., and Scheuchl, B.: Ice-shelf melting around Antarctica., Science, 341, 266–70, doi:10.1126/science.1235798, 2013.

Rosenau, R., Schwalbe, E., Maas, H.-G., Baessler, M., and Dietrich, R.: Grounding line migration and high-resolution calving dynamics of Jakobshavn Isbrae, West Greenland, Journal of Geophysical Research: Earth Surface, 118, 382–395, doi:10.1029/2012JF002515, 2013.

Schoof, C.: Ice sheet grounding line dynamics: Steady states, stability, and hysteresis, Journal of Geophysical Research, 112, F03S28, doi:10.1029/2006JF000664, 2007.

Seroussi, H., Morlighem, M., Rignot, E., Larour, E., Aubry, D., Ben Dhia, H., and Kristensen, S. S.: Ice flux divergence anomalies on 79north Glacier, Greenland, Geophysical Research Letters, 38, doi:10.1029/2011GL047338, l09501, 2011.

Seroussi, H., Morlighem, M., Larour, E., Rignot, E., and Khazendar, a.: Hydrostatic grounding line parameterization in ice sheet models, The Cryosphere, 8, 2075–2087, doi:10.5194/tc-8-2075-2014, 2014.

Sethian, J.: Evolution, Implementation, and Application of Level Set and Fast Marching Methods for Advancing Fronts, Journal of Computational Physics, 169, 503–555, doi:10.1006/jcph.2000.6657, 2001.

Sohn, H.-G., Jezek, K. C., and van der Veen, C. J.: Jakobshavn Glacier, west Greenland: 30 years of spaceborne observations, Geophysical Research Letters, 25, 2699–2702, doi:10.1029/98GL01973, 1998.

Truffer, M. and Echelmeyer, K. a.: Of isbrae and ice streams, Annals of Glaciology, 36, 66–72, doi:10.3189/172756403781816347, 2003.
van der Veen, C., Plummer, J. C., and Stearns, L. A.: Controls on the recent speed-up of Jakobshavn Isbræ, West Greenland, Journal of Glaciology, 57, 770–782, doi:10.3189/002214311797409776, 2011.
Vieli, A. and Nick, F. M.: Understanding and Modelling Rapid Dynamic Changes of Tidewater Outlet Glaciers: Issues and Implications, Surveys in Geophysics, 32, 437–458, doi:10.1007/s10712-011-9132-4, 2011.
Weertman, J.: Stability of the junction of an ice sheet and an ice shelf, Journal of Glaciology, 13, 3–11, 1974.
Winkelmann, R., Martin, M. a., Haseloff, M., Albrecht, T., Bueler, E., Khroulev, C., and Levermann, a.: The Potsdam Parallel Ice Sheet Model (PISM-PIK) – Part 1: Model description, The Cryosphere, 5, 715–726, doi:10.5194/tc-5-715-2011, 2011.
Zhao, H.-K., Chan, T., Merriman, B., and Osher, S.: A variational level set approach to multiphase motion, Journal of computational physics, 127, 179–195, 1996.
Zwally, H. J., Jun, L., Brenner, A. C., Beckley, M., Cornejo, H. G., Dimarzio, J., Giovinetto, M. B., Neumann, T. a., Robbins, J., Saba, J. L., Donghui, Y., and Wang, W.: Greenland ice sheet mass balance: distribution of increased mass loss with climate warming; 2003–07 versus 1992–2002, Journal of Glaciology, 57, 88–102, doi:10.3189/002214311795306682, 2011.

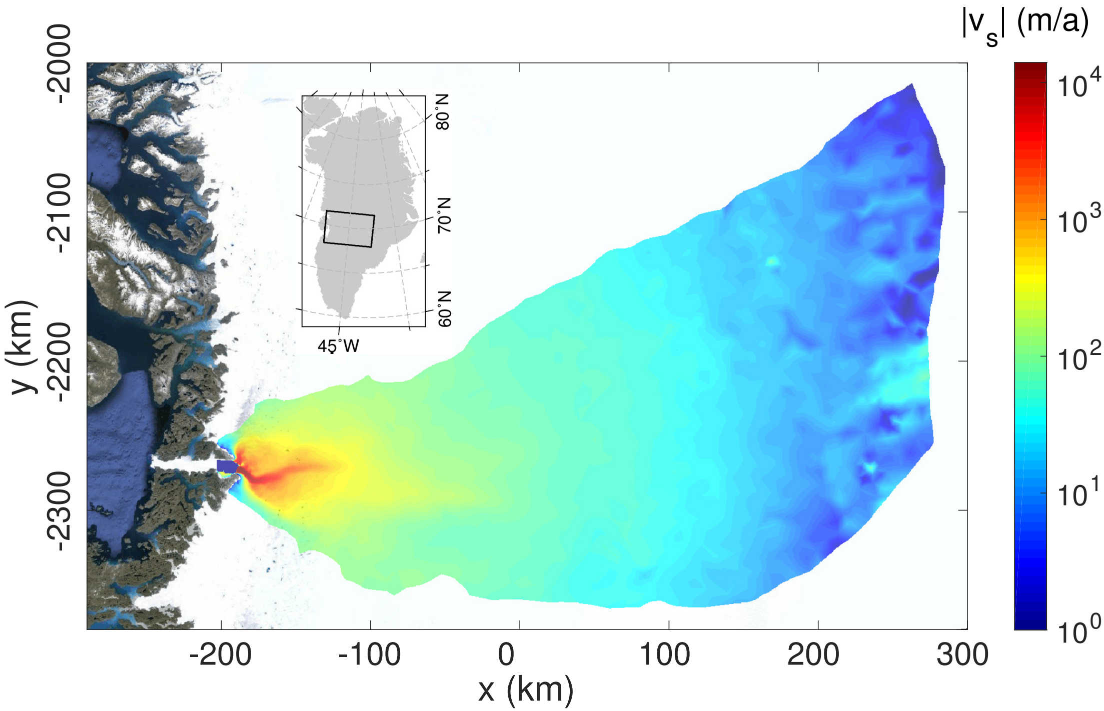

Figure 1. Observed ice surface velocities 2008/2009 (Rignot and Mouginot, 2012) of the Jakobshavn Isbræ drainage basin ~~used for modelling~~ (logarithmic scale). Background image from Google Earth ©.

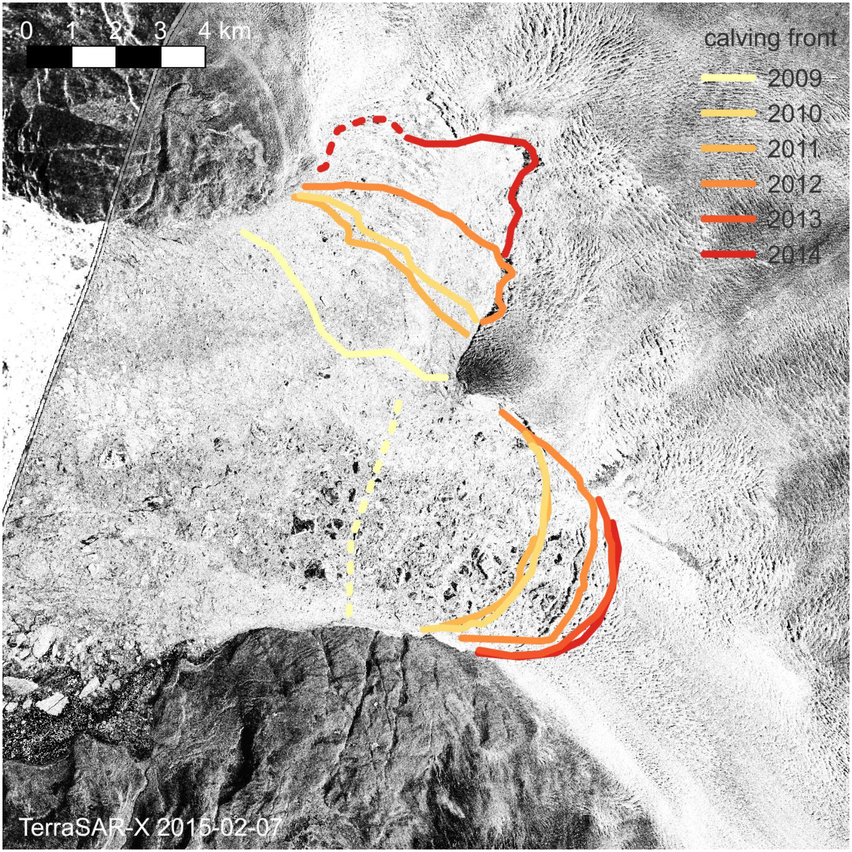

Figure 2. Winter (Feb-Mar) ~~ice~~ calving front positions from 2009 to 2014 ~~superimposed~~ overlaid on a TerraSAR-X scene from 2015-02-07 (© DLR). ~~Striped~~ Dashed lines are used in case of ambiguous ~~ice~~ calving front positions.

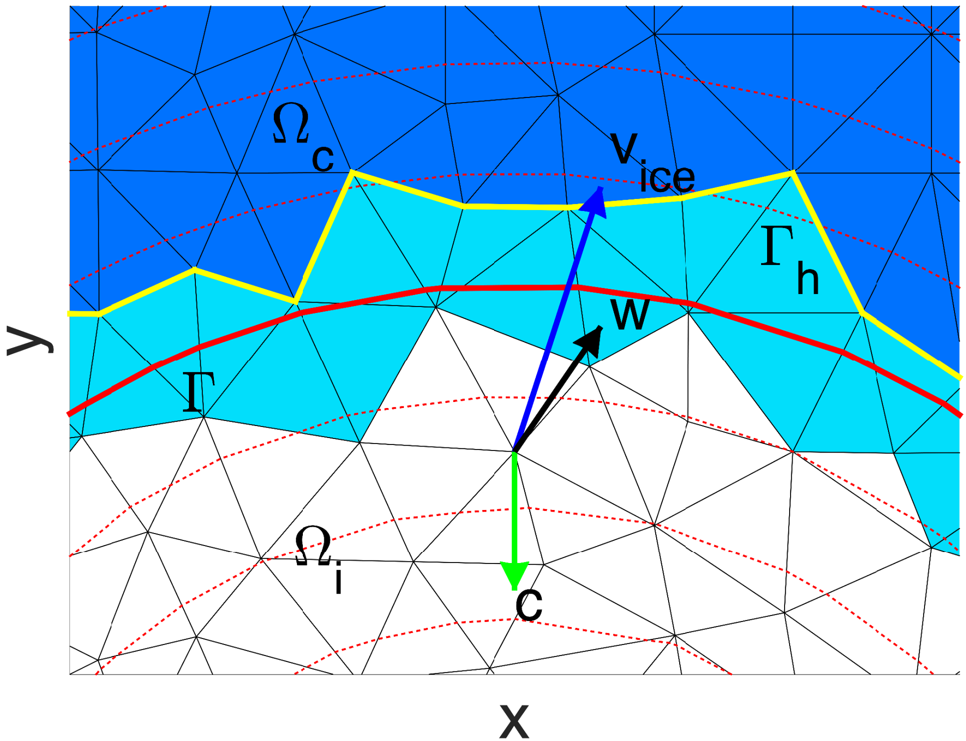

Figure 3. Schematic of the numerical ice margin. The red dashed lines denote different contour lines (level-sets) of the LSF φ. The thick red line marks the ~~zero level-set~~0-level-set, Γ, the yellow ~~one~~ line the numerical ~~ice~~ calving front Γ^{h}. ~~Blue~~ Dark blue triangles are ice-free elements, white ones ~~the~~ are ice-filled ~~ones~~ and ~~green~~ the light blue ones are the front elements. The three vectors show an example of the level-set velocity $\boldsymbol{w} = \boldsymbol{v} + \boldsymbol{c}$ at a finite element node.
~~The three vectors show an example of the evaluation of the boundary velocity~~ ~~$\boldsymbol{w}$~~ ~~at a finite element node.~~

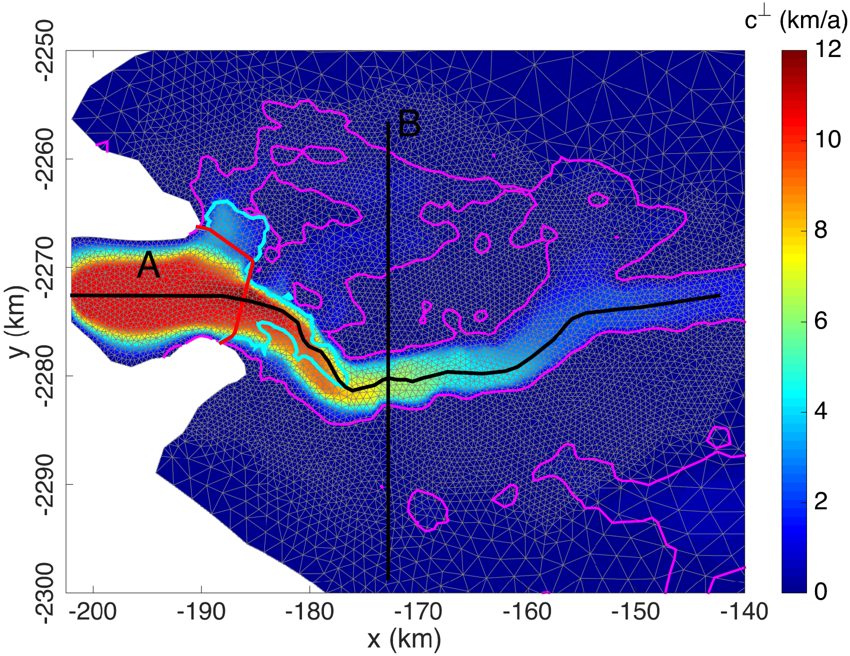

Figure 4. ~~The applied calving~~ Calving rate field $c_0^{\perp}$ in the region of fast flow, which has been derived from modelled ice velocities at the end of the ~~geometry~~ relaxation run. The red line indicates the ~~zero level-set~~ 0-level-set of the initial LSF used for geometry relaxation and as start position for the ~~ice~~ calving front during the experiments. The turquoise line marks the grounding line. Purple contours indicate zero bedrock elevation. Black lines are the ~~tracks~~ “along-trough” (A) and “across-trough” (B) profiles used in Fig. 6. The ~~start points of tracks A and B are the western and northern end, respectively. The~~ finite element mesh is displayed in grey.

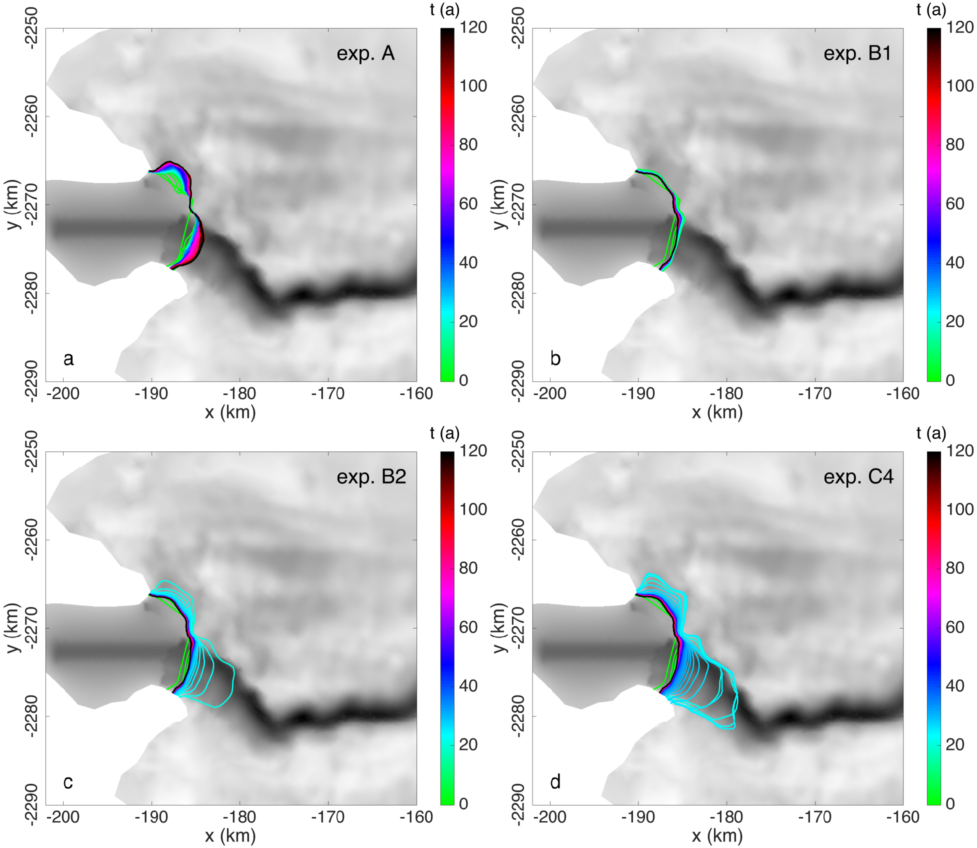

Figure 5. ~~Ice~~ Calving front ~~position~~ positions for experiments A, B1, B2 and C4 at the start of each year, plotted over basal topography (grey).

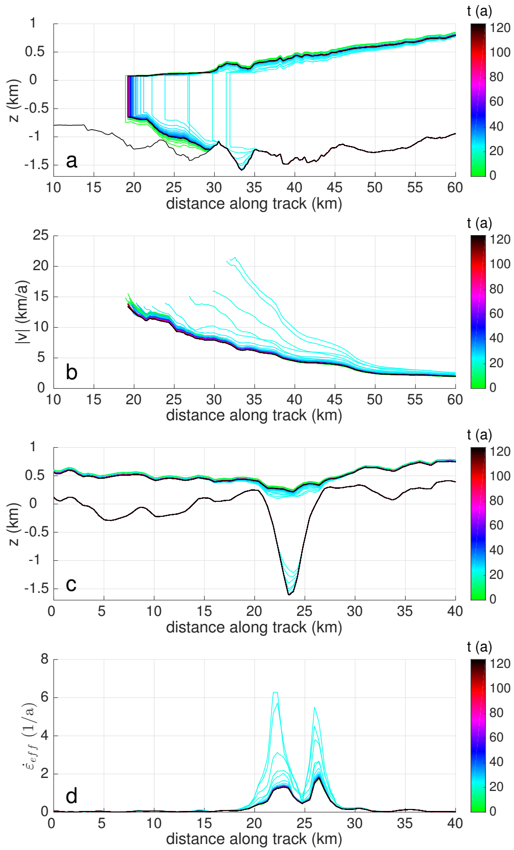

Figure 6. Section ~~values of~~ profiles for experiment C4 at the end of the calving season in October each year. a) ice geometry and b) ice velocity along-trough. c) ice geometry and d) effective strain rates across-trough. Positions of the ~~tracks~~ lines are given in Fig. 4.

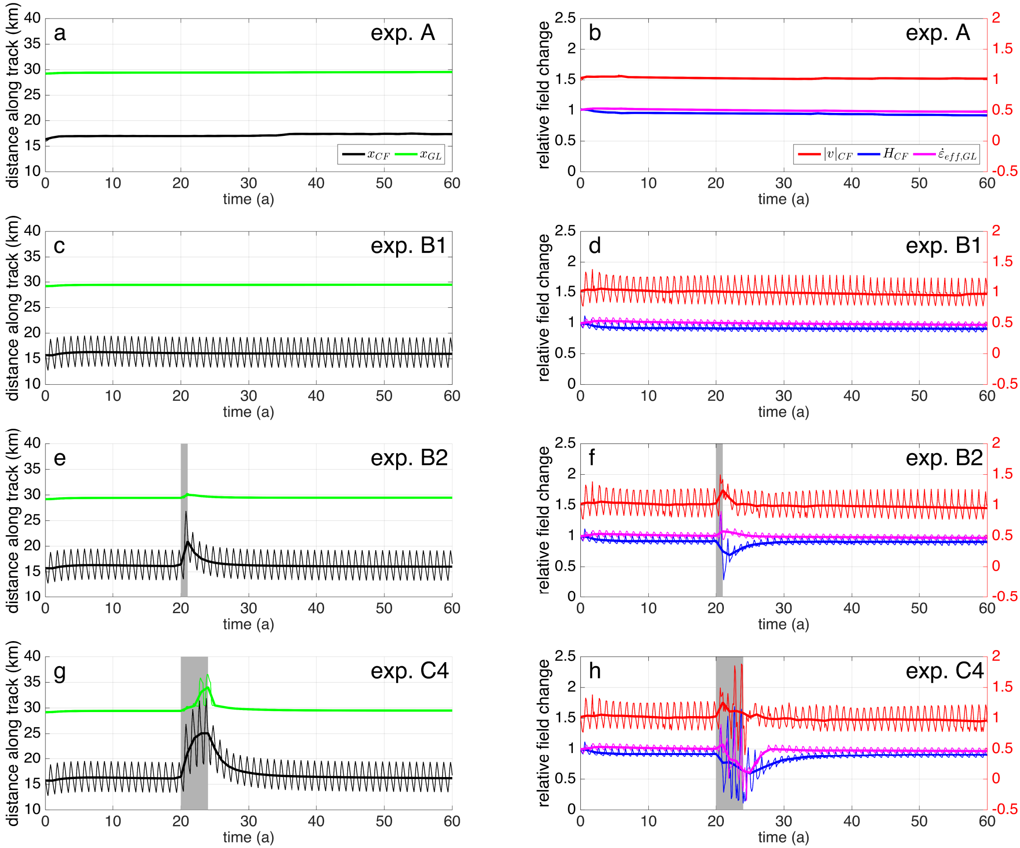

Figure 7. ~~Ice~~ Calving front and grounding line ~~position~~ positions along-trough (left column), ~~as well as values of ice~~ calving front thickness, ice velocity and effective strain rate relative to their initial value along-trough (right column) over time for experiments ~~a)~~ A, ~~b)~~ B1, ~~c)~~ B2 and ~~d)~~ C4. Perturbation intervals are marked in grey. Relative values for ice velocity ~~has~~ have been shifted up by 0.5 ~~up~~ for better visibility (red y-axis).

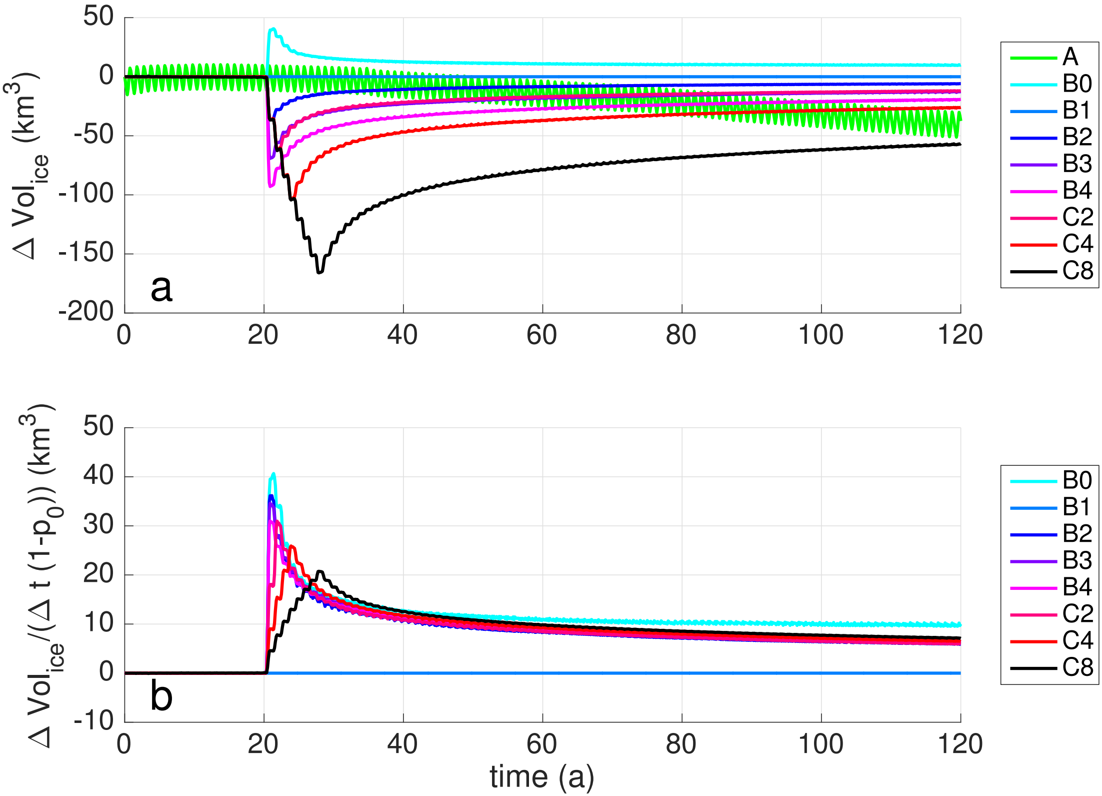

Figure 8. ~~Difference~~ a: Absolute difference in ~~total~~ ice volume ~~of~~ for the different simulations with respect to experiment B1~~over time~~. The ~~smooth~~ non-oscillating ice volume profile of experiment A causes its difference to experiment B1 to oscillate. b: The volume differences from experiments B and C divided by $\Delta t(1-p_0)$, the measure of the time-integrated calving rate perturbation.

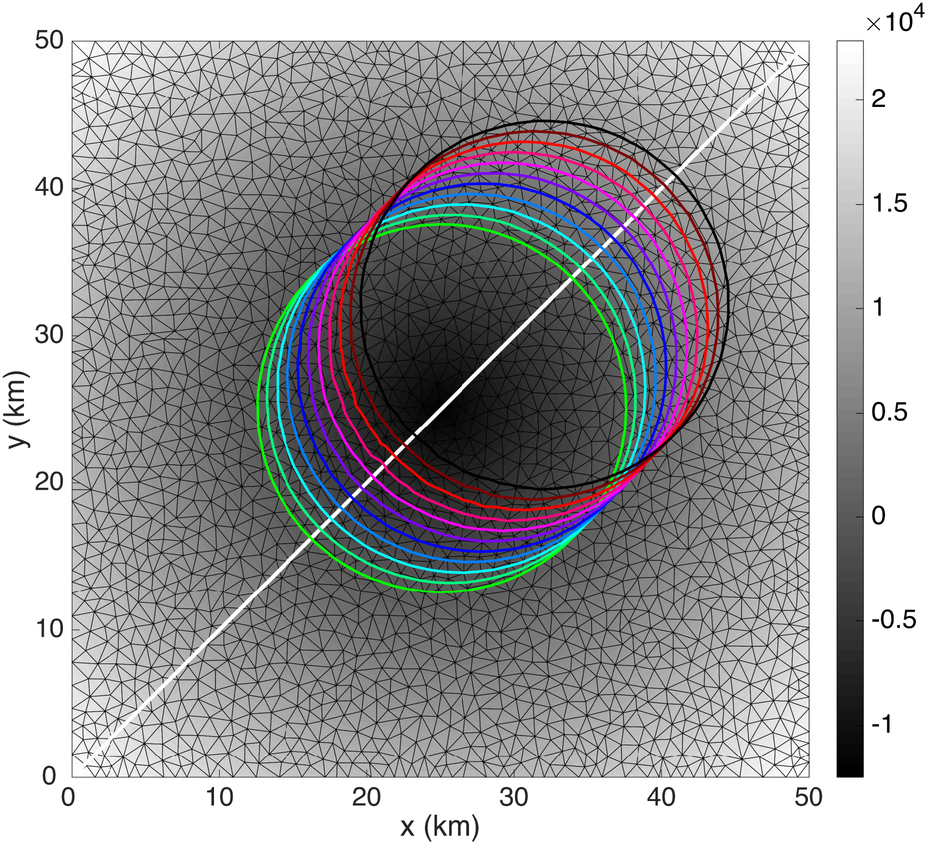

Figure 9. ~~0-level-set position~~ Zero-level-set positions at the start of every year, plotted over φ_0, which is ~~shaded~~ in grey scale. An example of the mesh with element size 1 km is marked in black. The white diagonal marks the ~~straight~~ line along which the velocity of the 0-level-set is tracked.

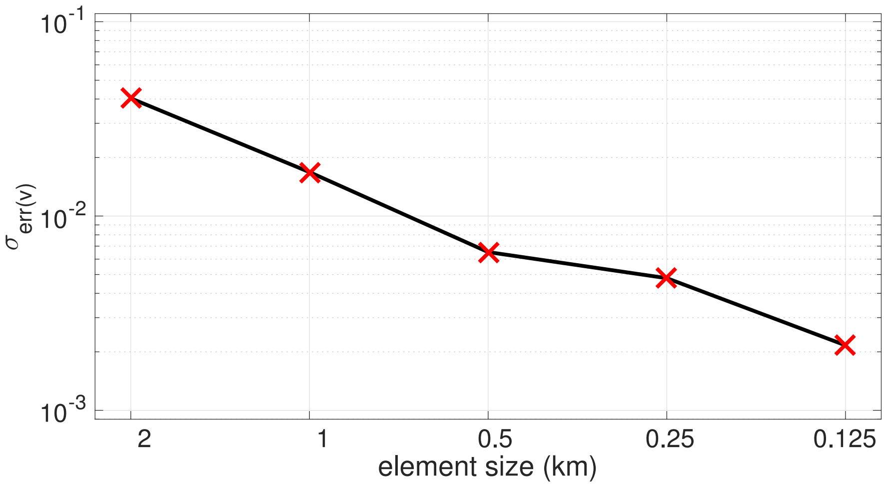

Figure 10. Standard deviation of the relative numerical error in advection velocity of the 0-level-set depending on mesh element size.

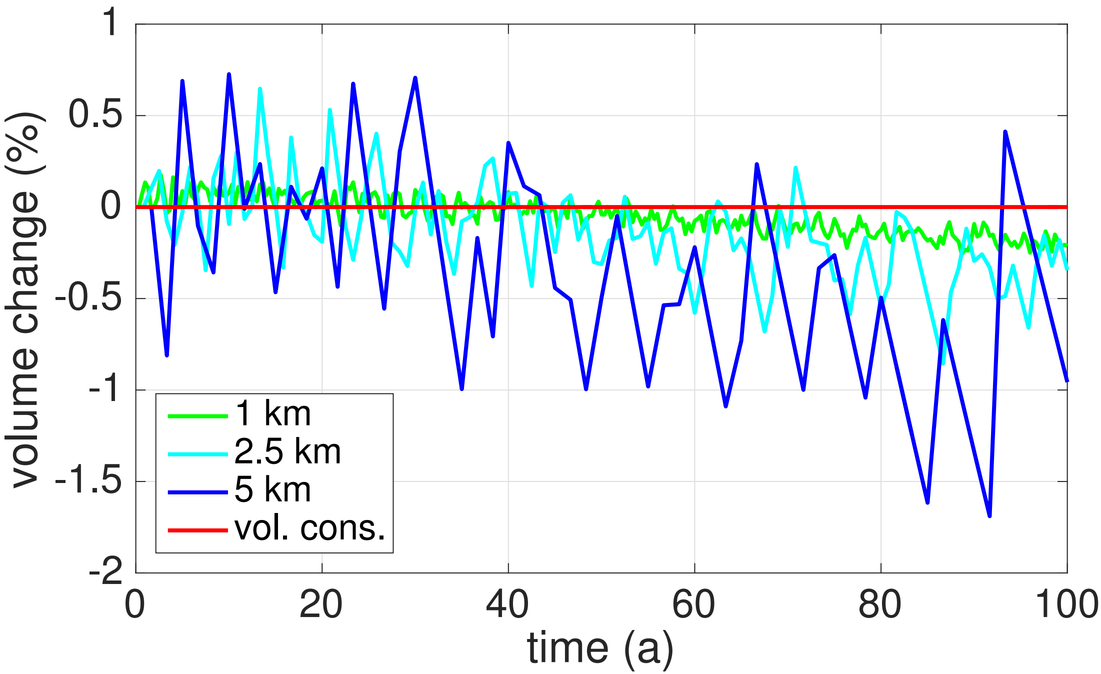

Figure 11. Evolution of the relative ice volume change for different element sizes. The red line shows volume conservation.

Table 1. Symbols and model parameters

Symbol	Quantity
μ	Ice viscosity
B	Ice viscosity parameter
$\dot{\varepsilon}_e$	Effective strain rate
n	Glen's flow law parameter
α	Basal friction parameter
N	Effective basal pressure
$\boldsymbol{v}$	Depth-averaged horizontal ice velocity
H	Ice thickness
a_s	Surface mass balance
a_b	Basal mass balance
Ω	Computational domain
Ω_i	Ice domain
~~$\Omega_\mathrm{i}^\mathrm{h}$ Numerical ice domain~~ Ω_c	Ice free domain
Γ	Ice boundary
Γ^h	Numerical ice boundary
φ	Level-Set Function
$\boldsymbol{n}$	Unit surface normal ~~on Γ~~
$\boldsymbol{w}$	~~Ice front~~ Level-set velocity
$\boldsymbol{a}$	Ablation velocity
$a^\perp$	Ablation rate
$\boldsymbol{c}$	Calving velocity
$c^\perp$	Calving rate
s	Scaling function
p	Perturbation function
Δt	Perturbation duration
p_0	Perturbation strength
L	Seasonal calving period length
ϕ_0	Phase shift
~~P Perturbation measure~~ Q_cf	Calving flux

Table 2. Table of experiments

Name	p_0	Δt	Name	p_0	Δt	Name	p_0	Δt
A	1	0	B2	2	1	C2	2	2
B0	0	1	B3	3	1	C4	2	4
B1	1	1	B4	4	1	C8	2	8